FLORIDA DEPARTMENT OF TRANSPORTATION

Research Progress Report
Use of Infrared Thermography for the Inspection of Welds in the Shop and Field

Final Report

FDOT BDV31-977-64

December 2017

Dr. Michele V. Manuel, Chair and Professor
University of Florida, Department of Materials Science and Engineering

Dr. Glenn Washer, Professor
University of Missouri, Department of Civil and Environmental Engineering

DISCLAIMER PAGE

The opinions, findings, and conclusions expressed in this publication are those of the authors and not necessarily those of the State of Florida Department of Transportation.

METRIC CONVERSION CHART

Conversion to SI units

SYMBOL	WHEN YOU KNOW	MULTIPLY BY	TO FIND	SYMBOL
LENGTH				
in	inches	25.4	millimeters	mm
ft	feet	0.305	meters	m
yd	yards	0.914	meters	m

SYMBOL	WHEN YOU KNOW	MULTIPLY BY	TO FIND	SYMBOL
AREA				
in^2	square inches	645.2	square millimeters	mm^2

SYMBOL	WHEN YOU KNOW	MULTIPLY BY	TO FIND	SYMBOL
MASS				
lb	pounds	0.454	kilograms	kg

SYMBOL	WHEN YOU KNOW	MULTIPLY BY	TO FIND	SYMBOL
TEMPERATURE (exact degrees)				
^oF	Fahrenheit	5 (F-32)/9 or (F-32)/1.8	Celsius	^oC

SYMBOL	WHEN YOU KNOW	MULTIPLY BY	TO FIND	SYMBOL
FORCE and PRESSURE or STRESS				
lbf	poundforce	4.45	newtons	N
lbf/in^2	poundforce per square inch	6.89	kilopascals	kPa

APPROXIMATE CONVERSIONS TO SI UNITS

SYMBOL	WHEN YOU KNOW	MULTIPLY BY	TO FIND	SYMBOL
LENGTH				
mm	millimeters	0.039	inches	in

m	meters	3.28	feet	ft

SYMBOL	WHEN YOU KNOW	MULTIPLY BY	TO FIND	SYMBOL
AREA				
mm^2	square millimeters	0.0016	square inches	in^2
m^2	square meters	10.764	square feet	ft^2

SYMBOL	WHEN YOU KNOW	MULTIPLY BY	TO FIND	SYMBOL
MASS				
g	grams	0.035	ounces	oz
kg	kilograms	2.202	pounds	lb

*SI is the symbol for the International System of Units. Appropriate rounding should be made to comply with Section 4 of ASTM E380.

Technical Report Documentation Page

1. Report No.	2. Government Accession No.	3. Recipient's Catalog No.
4. Title and Subtitle Use of Infrared Thermography for the Inspection of Welds in the Shop and Field		5. Report Date December 28, 2017
		6. Performing Organization Code
7. Author(s) Drs. Michele Manuel and Glenn Washer		8. Performing Organization Report No.
9. Performing Organization Name and Address University of Florida 152 Rhines Hall 549 Gale Lemerand Drive Gainesville, Florida 32611		10. Work Unit No. (TRAIS)
		11. Contract or Grant No. BDV31-977-64
12. Sponsoring Agency Name and Address Florida Department of Transportation 605 Suwannee Street, MS 30 Tallahassee, FL 32399		13. Type of Report and Period Covered Final Report January 2017 – January 2018
		14. Sponsoring Agency Code
15. Supplementary Notes		

16. Abstract

This report represents an initial, proof-of-concept study to explore the feasibility of infrared ultra-time domain (IR-UTD) technology for the detection of defects in welds. The report includes two primary sections. The first section provides some background on the technology of infrared thermography (IRT) and common methods of applying that technology for the detection of defects in materials. This includes a summary of previous research found in the literature that applies to the detection of defects in steel welds using IRT. A second, experimental section explores the use of IRT on various specimens using several excitation sources to image subsurface defects. Progress was made and subsurface targets could be detected. It is envisioned that the successful completion of this work will open the opportunity for a larger analytical study to quantify IRT images with specific flaw types and geometries that are detrimental to mechanical integrity of the weld.

17. Key Word	18. Distribution Statement
Thermography, Welds, IR-UTD	No restrictions.

19. Security Classif. (of this report)	20. Security Classif. (of this page)	21. No. of Pages	22. Price
Unclassified.	Unclassified.	44	

Form DOT F 1700.7 (8-72) Reproduction of completed page authorized

EXECUTIVE SUMMARY

This report contains experimental testing of the infrared ultra-time domain (IR-UTD) imaging technology as applied to defects in steel. It was found that the previous literature on the application of infrared thermography (IRT) for the detection of defects in steel welds is limited; however, previous research on metal components demonstrates that there is potential for developing this unique application of IRT. Almost 50 separate tests have been completed, and a variety of different processing approaches were attempted, including the use of various excitation sources to improve the imaging of subsurface defects in steel. Several different specimens were produced to support the testing procedures. Progress was made and shallow subsurface target defects were detected in some cases. Surface-breaking cracks were found to produce detectable indications using the IR-UTD technology. Analysis of the potential for using IRT for the inspection of welds in steel members and recommendations for future research to further develop the technology toward implementation are provided.

Table of Contents

List of Figures

List of Tables

1. Chapter 1 – Introduction

1.1. Motivation

The fabrication of steel bridge members typically consists of welding plates together to form a structural shape and/or to provide for increased cross-section (i.e., transitions in plate width or thickness). The durability and strength of the fabricated bridge member relies on the quality of the welding process. Flaws or defects can be produced during the welding process that undermine the strength and durability of the weld and therefore the bridge member itself (McGonnagle, 1956; Shenefelt, 1971). Quality control procedures are used during the fabrication process to identify flaws and defects, such that repairs can be implemented (AWS 2010). These procedures include the application of nondestructive evaluation (NDE) technologies to identify subsurface weld flaws such at porosity in the weld, lack of fusion, slag inclusions, and cracks.

Conventional NDE methods for ensuring weld quality include the use of radiographic testing (RT) and ultrasonic testing (UT). Radiographic testing creates indications due to variations in density resulting from a defect in the weld material. Ultrasonic testing responds to discontinuities in the material that reflect an acoustic wave (Kinzel *et al.,* 1929; McGonnagle, 1956).

Radiographic testing of welds requires radiographic source exposure such that safety steps are needed to separate the RT process from human interaction. This may include removing a member from the production line to a separate location in the shop, for production to be stopped and lead shields installed to protect shop personnel, or for images to be produced during the third-shift when the shop has reduced manpower. For this reason, the use of RT reduces the efficiency of the fabrication process and increases costs. Despite this limitation, RT is often preferred by owners because images are produced that document the weld quality for review, quality assurance, and archival records (Rezai *et al.*, 2005).

Ultrasonic testing is sensitive to defects such as cracks and lack of fusion in welds, but less sensitive to volumetric defects such as slag inclusion, voids, or porosity. The use of UT can be complicated and relies heavily on the quality of the inspector conducting the testing (Washer *et al.*, 2014). Testing requires an ultrasonic transducer to be scanned over the surface of the specimen after the plate has cooled from the welding process. This scanning procedure can be influenced by human factors that reduce the reliability of the process. Ultrasonic testing reports typically document indications detected in the weld (i.e., discontinuities that result in the reflection of the acoustic wave), and therefore limited information on the quality of the welds is available for review, quality assurance, and archival records.

These traditional NDE technologies have been successful in ensuring quality during the fabrication process, but have limitations as described above. Infrared thermography (IRT) has the potential to provide some of the best features of RT and UT while improving the efficiency of the inspection process in the fabrication shop. Infrared thermography typically produces images representing the surface temperature of the

material under inspection; subsurface flaws in the material can affect the heat transfer properties and result in surface temperature anomalies. These surface temperature anomalies are interpreted as defects or flaws in the material. In this way, infrared thermography has the potential to produce an image of internal weld flaws similar to RT, without the health safety concerns. Additionally, using the heat from the welding process to produce surface temperature anomalies has the potential to allow for IRT to be implemented in the production line, without waiting for the material to cool fully (as is required for UT). In addition, because the IR technology produces images of the surface of the weld, quality measures typically assessed through visual inspections by certified weld inspectors (CWIs) may be possible using the image produced from IRT. In this way, the use of IRT could reduce costs and improve the efficiency of steel bridge fabrication.

The objective of the project was to evaluate the feasibility of using advanced IRT for inspection of weld quality. To achieve this objective, a description of prior research regarding the suitability of using IRT for weld inspection was included. Furthermore, parameters such as time required, accuracy, and types of flaws that could be detected were evaluated experimentally through proof-of-concept testing.

However, there are some challenges with using traditional IRT for detecting weld flaws. For materials such as concrete, which have relatively low thermal conductivity, temperature variations produced from diurnal temperature changes have been used to detect subsurface delamination. However, in a metal, the conductivity is significantly higher, and as a result, traditional IRT is not capable of imaging surface temperature variations resulting from subsurface damage. New IRT technologies have been developed in the last 5 years that image the thermal inertia of the material, rather than simply the surface temperature (Fuchs, 2014; Washer *et al.,* 2016). Fabrication-related heating and cooling processes, such as the cooling of the steel immediately following the welding process, may provide the necessary thermal gradients to detect subsurface damage using thermal inertial measurements. The new IRT technologies, known generally as infrared ultra time-domain (IR-UTD) imaging, has demonstrated ability to provide more accurate imaging of subsurface flaws in concrete, and to detect typical coating defects in steel members (e.g. lack of adhesion or corrosion under coatings). Detection of coating defects in metalized coatings has also been demonstrated. The proposed research was intended to explore the application of these new technologies for the detection of weld flaws. Application of the advance IRT technology for fabrication inspection could improve efficiency and reduce fabrication costs.

1.2. Project Objective

The objective of the project was to evaluate the feasibility of using advanced IRT technologies for inspection of weld quality. The effort represented an initial, proof-of-concept study to explore the feasibility of IR-UTD technology for the detection of defects in welds. It is envisioned that the successful completion of this work will open the opportunity for a larger analytical study to quantify IRT images with specific flaw types and geometries that are considered to be detrimental to mechanical integrity of the weld.

2. Chapter 2 - Background

Infrared thermography is a technology that images the emission of thermal energy from the surface of a material. A common application of the technology is to convert the thermal flux detected by the camera to an estimate of the surface temperature of the object being observed. Such thermal images are commonly used in a wide range of applications such as detecting damaged electrical components, security applications, and detecting damage in concrete structures. These applications utilize passive thermography, in which thermal variations are created either by the performance of equipment itself or its surrounding environment. For example, electrical transformers exhibit increased heating if they are damaged or near the end of their service lives. This increase in temperature can be detected using a thermal camera. For concrete components, subsurface damage such as areas of delamination caused by corrosion can disrupt thermal transfer through the material. Diurnal temperature variations in the environment surrounding the concrete cause the material to heat and cool over a 24 hr time interval. Areas where heat transfer is disrupted by subsurface delamination manifest in anomalies in the surface temperature measured by the thermal camera. Figure 2-1 shows an area of delamination in concrete imaged by a thermal camera. In the figure, a subsurface delamination in the concrete appears as a hot-spot on the surface of the material, and this hot-spot is revealed in the thermal image.

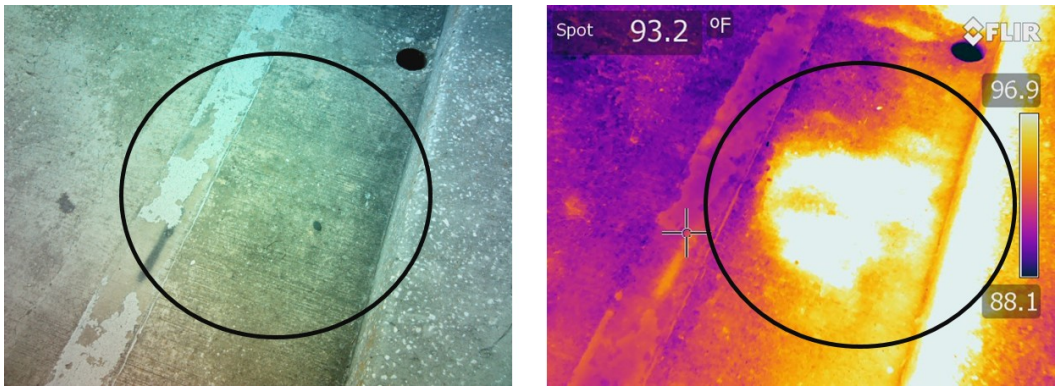

Figure 2-1. Photograph (left) and thermal image (right) revealing a subsurface defect in a bridge deck.

Active thermography is a process in which an outside heating (or cooling) source is used to impart thermal variations an object. Typically this involves heating the object such that thermal anomalies can be observed as the object returns to thermal equilibrium with its surrounding environment (Maldague, 2000). There are several forms of active thermography that have been developed in the past, many developed for the detection of subsurface defects in composite materials. These can generally be characterized as pulsed thermography (PT), sometimes called flash thermography, and lock-in thermography (LT).

Pulsed (or flash) thermography utilizes a flash of intense heat, such as that produced by a quartz flash lamp, to provide a sudden heat input on the surface of a material. The

thermal wave produced diffuses into the material, and this process is observed using a thermal camera. Anomalies or defects in the material will affect the diffusion of heat into the material, and the anomalies can be detected by processing several thermal images captured during the cooling cycle. Typically, each pixel of the IR image from a series of thermal images is analyzed during the cooling of the object. Characteristics such as the rate of cooling and the phase (timing) of the cooling for intact areas as compared with damaged areas can be analyzed.

In some cases, data is processed using one-dimensional Fourier transformation (FFT) resulting in both amplitude and phase images (Ibarra-Castanedo *et al.*, 2009). This method of processing the data from a PT application is commonly referred to as pulsed phase thermography (PPT). This approach to processing data is used because the phase images are less influenced by surface characteristics, such as variations in surface color, texture, or geometry (Maierhofer *et al.*, 2006; Ibarra-Castanedo *et al.*, 2009). The amplitude images offer increased depth information. Improved results can be obtained from processing the data in this manner, at the expense of increased complexity and additional post-processing requirements.

Another approach to active thermography is LT. The principle of LT is to induce a sinusoidal heat source at the surface of the material and analyze the resulting thermal wave that propagates throughout the material under test. Theoretically, LT works by inducing a sinusoidal heating on the surface of the specimen and analyzing the resulting surface temperature variations as shown in Figure 2-2. The sinusoidal surface temperature variations can be described in one-dimension:

$$T(i,j) = Ae^{i[\omega t - \varphi(i,j)]}$$

Where A is the thermal wave amplitude and $\varphi(i,j)$ is the phase. The surface temperature field can be reconstructed by extracting thermal data for individual pixels at quadrature points in the sinusoidal wave. The resulting calculations for the phase and the amplitude of the temperature field are (Choi *et al.*, 2008):

$$\varphi(i,j) = \ tan^{-1}\left(\frac{S_1(i,j) - S_3(i,j)}{S_2(i,j) - S_4(i,j)}\right)$$

$$A(i,j) = \sqrt{\left(S_1(i,j) - S_3(i,j)\right)^2 - \left(S_2(i,j) - S_4(i,j)\right)^2}$$

Where $S_n(i,j)$ are individual thermal images captured at different points in time during the thermal cycle, as shown in Figure 2-2. Performing these calculations for each pixel in the image results in the creation of amplitude and phase images. This calculation is simple and relatively fast, but can be negatively affected by noise in the thermal signal; noise can be mitigated by averaging several pixels as illustrated in Figure 2-2.

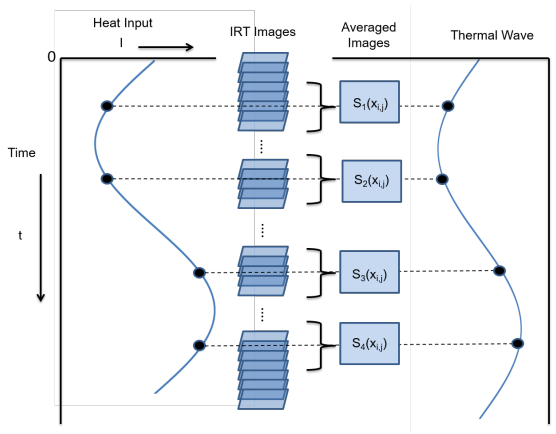

Figure 2-2 Schematic illustration of LT processing.

The primary difference between PT and LT is the use of a modulated heat source that provides a repetitive thermal wave propagating through the material. In this way, the phase and amplitude variations from numerous cycles can be combined to provide improved signal-to-noise ratios.

Ultra-time domain (UTD) thermal imaging combines the data processing approaches used in the active thermography with the ambient temperature variations that occur naturally in the environment. As such, this new technology is a combination of the thermal excitation methods used in passive thermography with the data processing used in active thermography such as PT and LT. In this way, improved imaging capabilities can be achieved relative to conventional, passive applications. During this research, the UTD technologies, as well as PT and LT, approaches are being utilized to determine the feasibility of using these techniques for the inspection of welds in steel bridges.

3. Chapter 3 - Experimental Methods

This portion of the report describes the experimental test arrangements that were used to develop methodologies for detecting flaws in welds. The initial experiments were completed on a weld specimen with embedded flaws. Tests were also completed on steel plate specimens with cut-outs to represent flaws as a development tool for the technology. Different heating sources were also used as described below. A specialized test frame was constructed to provide a stable platform for developmental testing.

3.1. Experimental Approach

The objective of the research was to evaluate the feasibility of advanced IRT technologies for inspection of weld quality. As discussed in Chapter 2, advanced IRT methods include different approaches such at PT, LT and IR-UTD. Each of these approaches utilizes time-lapse thermal images captured during heating and cooling process to detect subsurface defects. The different approaches process data differently, and may use different excitation methods for producing heating and cooling. Each of these different methods were evaluated through laboratory testing in an effort to determine the feasibility of detecting defects in welds. Testing was completed to identify procedures and methods that were likely to produce useful results when applied during welding processes in a fabrication shop.

Three test specimens were used during the course of the research, as described below. Specimen 1 was a specimen manufactured with actual defects in the weld. Additional specimens were fabricated as needed, based on initial tests that indicated subsurface flaws did not produce detectable indications. Generally, the additional specimens (Specimens 2 and 3) were produced with large simulated flaws intended to provide more easily detectable indications, from which suitable procedures for field application of the technology could be developed. Several different test setups and heating methods were also used in an effort to fully evaluate the feasibility of using advanced IRT for the detection of defects in welds.

3.2. Specimen I

Specimen I is a 12 x 17 x 1.25 in. plate with a butt weld containing three defects. The defects in Specimen I include a slag inclusion, lack of fusion, and cracking as shown in Figure 3-1. This uncoated test specimen included realistic weld flaws and a butt weld. The lack of fusion defect was 0.5 x 0.2 in. in dimension, located on the bevel 1.5 in. from the edge of the plate. The slag inclusion was located 4.0 in. from the edge of the plate at mid-depth and was 0.3 x 0.1 in. in dimension. A 0.4 in. long toe crack was located 8.8 in. from the edge of the plate, as shown in the figure. The toe crack extends from the surface to a depth of 0.15 in. Thermal images were captured of the surface of the specimen breached by the crack.

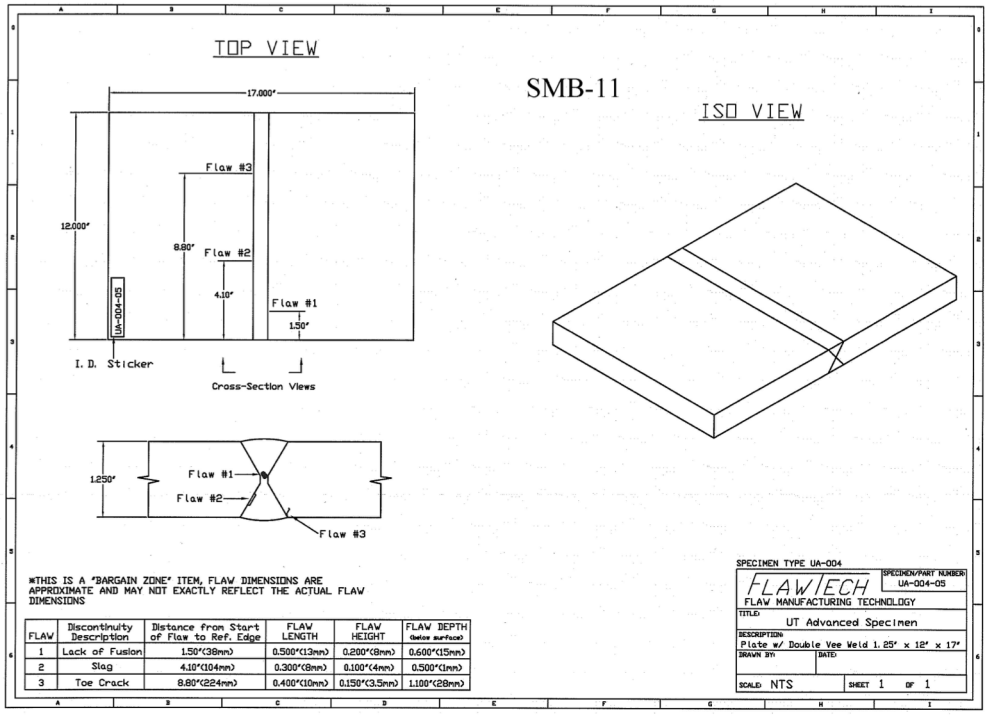

FLAW	Discontinuity Description	Distance from Start of Flaw to Ref. Edge	FLAW LENGTH	FLAW HEIGHT	FLAW DEPTH (below surface)
1	Lack of Fusion	1.50"(38mm)	0.500"(13mm)	0.200"(8mm)	0.600"(15mm)
2	Slag	4.10"(104mm)	0.300"(8mm)	0.100"(4mm)	0.500"(1mm)
3	Toe Crack	8.80"(224mm)	0.400"(10mm)	0.150"(3.5mm)	1.100"(28mm)

Figure 3-1. Specimen I design drawing showing type and location of defects in the weld.

3.3. Specimen II

Specimen II was a 36 x 28 x 1 in steel plate with a circular holes and linear slots cut into the plate. The purpose of Specimen II was to provide a test article containing simulated flaws for developing a methodology for imaging subsurface flaws in steel. The specimen included cut-outs of different sizes and depths as shown in Figure 3-2. The cut-outs in specimen II include slots and round holes. The slots measure 1 x 0.25 in., cut to different depths of 0.2, 0.4, 0.5 and 0.8 in. Flat-bottom holes (FBHs) with diameters of 0.25 and 0.5 in. were also cut into the plate with depths of 0.2, 0.4, 0.5 and 0.8 in. The large size of the plate was intended to reduce edge effects that can obscure images.

The plate was originally 36 x 56 in, and was later flame-cut to 36 x 28 in. for convenience. The surface of the specimen was coated with flat black paint to provide uniform and efficient emissivity from the surface.

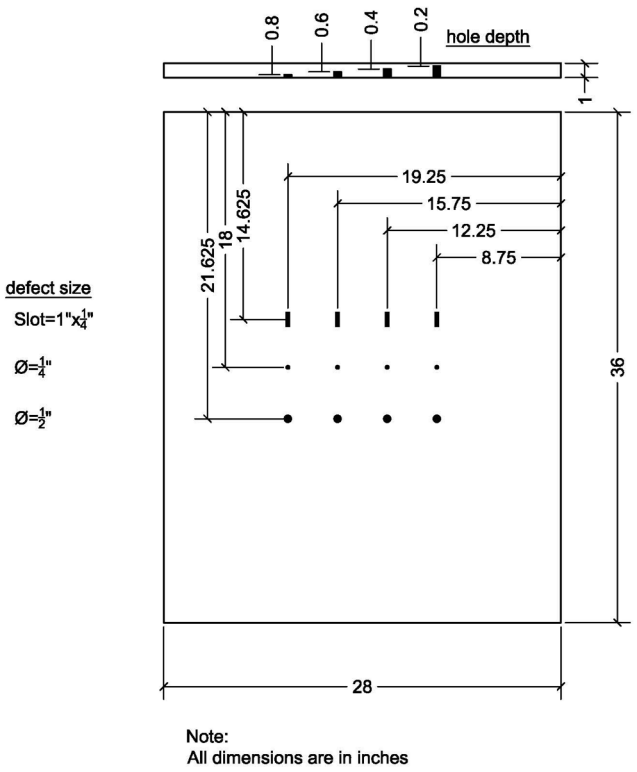

Figure 3-2. Specimen II design drawing showing type and location of defects in the weld.

3.4. Specimen III

Specimen III was a 16 x 12 x 0.25 in steel plate with circular cut-outs (i.e., FBHs). This specimen was produced to assist in the development of methodologies for imaging subsurface flaws in steel. The specimen included FBH with diameters of 0.25 and 0.5 in. The FBHs were cut to different depths from the surface of 0.05, 0.10, 0.15, and 0.20 in. as shown in Figure 3-3. The surface of the specimen was coated with flat black paint to provide uniform and efficient emissivity from the surface.

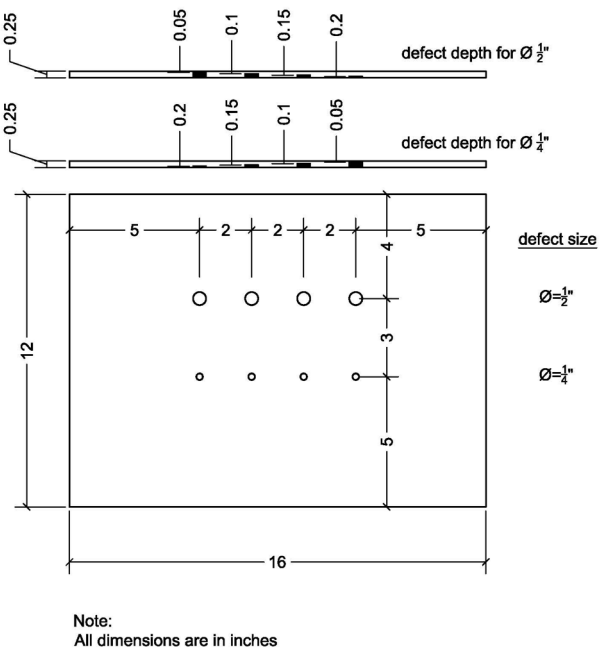

Figure 3-3. Specimen III design drawing showing type and location of defects in the weld.

3.5. Test Setups

Several different test setups were used during the course of the research. Test setup 1 consisted of mounting the thermal camera on a vertical mast with heating sources mounted above the specimen as shown in Figure 3-4. As shown in the figure, the specimen was placed on a riser to raise the specimen above the floor. IR heaters were

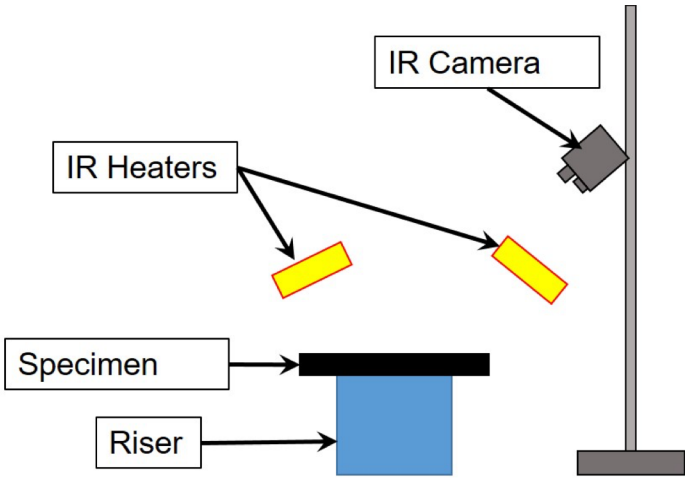

Figure 3-4. Schematic diagram of test setup 1.

suspended from the ceiling of the laboratory. The IR camera was mounted on a vertical mast that allowed the cameras to be placed at different elevations and with different angles relative to the surface of the specimen. This test arrangement was used to perform initial proof-of-concept testing.

Test setup 2 consisted of a test frame that was constructed to make testing more stable and systematic as shown in Figure 3-5. This test frame was constructed from aluminum sections with flexible mounting resources that enabled a number of different test arrangements to be implemented. The frame was designed such that the thermal camera could be mounted at a normal angle to the specimen being testing. The test frame also supported testing repeatability.

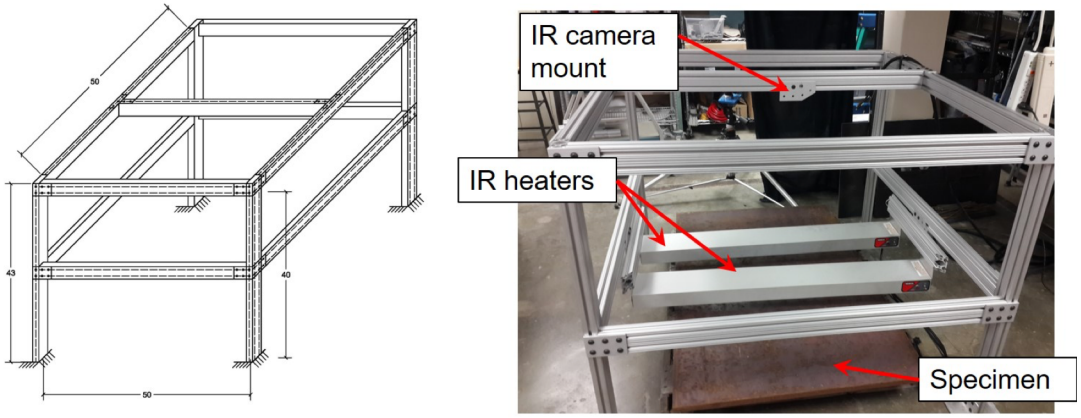

Figure 3-5. Drawing and photograph of test frame for test setup 2.

Test setup 3 was used to evaluate the application of directional heat to the specimen by mounting a resistive heater to the edge of the Specimen I, as shown in Figure 3-6. Thermocouples were also mounted on the plate to monitor surface temperatures during the testing. In this arrangement, the heat was imparted into the specimen from the edge of the plate and propagated normal to the weld axis. In this way, the directional heating of the weld is achieved, providing a thermal gradient across the plate. Flaws in the weld affect the flow of heat across the weld and disrupt the gradient. Heat transport from the center of the weld to each of the joined plates would provide a similar propagation pattern, albeit in the opposite direction.

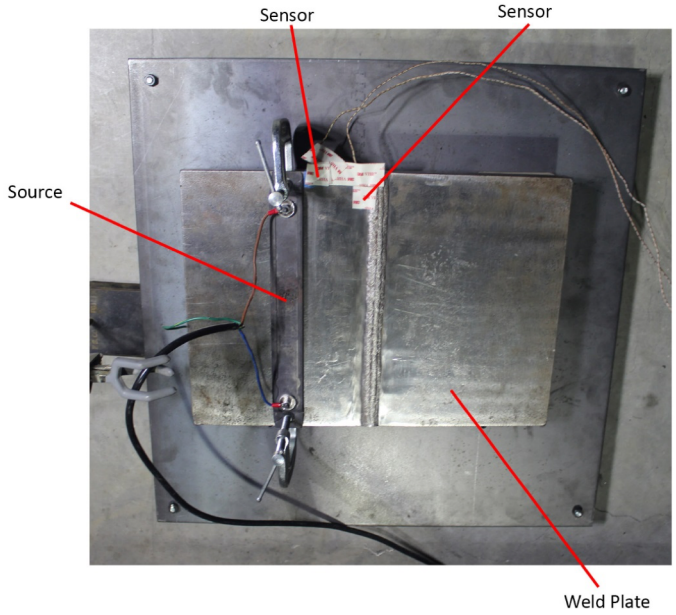

Figure 3-6. Photograph of specimen 1 with resistive heating element used for test setup 2.

3.6. Excitation Sources

Four different excitation sources were used to impart thermal energy into the specimen. A pair of industrial infrared heaters (1200 W) were used to provide a IR heating source for the specimens. A laboratory oven was also used to heat an entire specimen to 300°F. Propane heaters capable of producing 45,000 BTUs were used to provide a strong surface heating source. Finally, a resistive heating element was used in direct contact with the specimen to provide directional heating for differential measurements.

3.7. Test Procedures

Almost 50 separate tests were conducted using the different excitation sources and test arrangements previously described. Table 3-1 shows the different test parameters that have been explored. As shown in the table, different heating sources, heating intervals, data acquisition rates, and processing methods were used to evaluate the capabilities of advanced IRT for detecting defects in welds. Additional testing was completed to evaluate the feasibility of using advanced IRT for detection of defects in welds. These tests included the use of a thermal gradient produced from a resistive heater mounted on the surface of the plate.

Table 3-1. Summary of test procedures used to image subsurface flaws in steel specimen (UTD is an acronym for ultra-time domain and PPT is an acronym stands for pulsed phase thermography).

Spec.	Heating source	Data collection	Excitation frequency	# of images	Rate	Data processing
Specimen I	Electrical heaters	1 hr heating 45 min cooling	-	3,114	2 s	UTD
Specimen I	Electrical heaters	3 hrs heating 3 min cooling	-	365	30 s	UTD
Specimen I	Resistive heaters	2 min heating, 6 min cooling	-	50	-	UTD
Specimen I		Flash Therm.	-	-	-	UTD
Specimen II	Electrical heaters	1 hr cooling	-	30	2 min	PPT/UTD
Specimen II	Electrical heaters	15 min cooling	-	15	1 min	PPT/UTD
Specimen II	Electrical heaters	45 min cooling	-	45	1 min	PPT/UTD
Specimen II	Electrical heaters	-	5 min/5 min	60	1 min	PPT
Specimen II	Electrical heaters	-	10 min/10 min	80	1 min	PPT
Specimen II	Electrical heaters	-	10 min/10 min	60	1 min	PPT
Specimen II	Electrical heaters	-	3 min/3 min	60	1 min	PPT
Specimen II	Electrical heaters	-	2.5 min/2.5 min	60	1 min	PPT
Specimen II	Electrical heaters	-	3 min/3 min	180	1 min	PPT
Specimen II	Electrical heaters	-	10 min/10 min	200	2.5 min	PPT
Specimen II	Electrical heaters	-	10 min/10 min	180	1 min	PPT
Specimen II	Electrical heaters	3 hrs heating, 2 hrs cooling	-	166	2 min	PPT/UTD
Specimen II	Electrical heaters	1 hr heating, 1 hr cooling	-	240	30 s	PPT/UTD
Specimen II	Electrical heaters	1.5 hrs heating, 1.5 hrs cooling	-	1,081	10 s	PPT/UTD
Specimen II	Electrical heaters	-	1 min/1 min	720	5 s	PPT
Specimen II	Electrical heaters	51 min cooling	-	205	15 s	PPT/UTD

Spec.	Heating source	Data collection	Excitation frequency	# of images	Rate	Data processing
Specimen II	Electrical heaters	3 hrs heating, 2 hrs cooling	-	1,200	15 s	PPT/UTD
Specimen III	Electrical heaters	2 hrs heating, 2.5 hrs cooling	-	1,080	15 s	PPT/UTD
Specimen III	Electrical heaters	-	5 min/5 min	1,800	1 s	PPT
Specimen III	Electrical heaters	1 min cooling	-	240	0.25 s	PPT/UTD
Specimen III	Electrical heaters	75 s cooling	-	502	0.15 s	PPT/UTD
Specimen III	Electrical heaters	50 min heating, 1 hr cooling	-	6,600	1 s	PPT/UTD
Specimen III	Electrical heaters	-	10 min/10 min	1,600	1 s	PPT
Specimen III	Electrical heaters	1.5 hrs heating, 53 min cooling	-	8,577	1 s	PPT/UTD
Specimen III	Furnace	100 min cooling	-	6,002	1 s	PPT/UTD
Specimen III	Electrical heaters	-	20 min/20 min	3,406	1 s	PPT
Specimen III	Furnace	57 min cooling	-	3,426	1 s	PPT/UTD
Specimen III	Electrical heaters	-	10 s /10 s	801	0.15 s	PPT
Specimen III	Electrical heaters	-	60s / 60 s	601	1 s	PPT
Specimen III	Electrical heaters	10 min cooling	-	600	1 s	PPT/UTD
Specimen III	Furnace	10 min cooling	-	4,000	0.15 s	PPT/UTD
Specimen III	Gas heaters	30 min cooling	-	1,800	1 s	PPT/UTD
Specimen III	Gas heaters	35 min cooling	-	2,100	1 s	PPT/UTD
Specimen III	Gas heaters	9 min cooling	-	2,200	0.15 s	PPT/UTD
Specimen III	Gas heaters	-	10s /10 s	953	0.20 s	PPT
Specimen III	Gas heaters	7 min cooling	-	1,749	0.25 s	PPT/UTD
Specimen III	Gas heaters	8 min cooling	-	2,000	0.25 s	PPT/UTD

Table 3-1, continued

Spec.	Heating source	Data collection	Excitation frequency	# of images	Rate	Data processing
Specimen III	Gas heaters	15 min cooling	-	900	1 s	PPT/UTD
Specimen III	Gas heaters	42 min cooling	-	2,520	1 s	PPT/UTD
Specimen III	Gas heaters	30 min cooling	-	1,800	1 s	PPT/UTD

4. Chapter 4 - Results

4.1. Specimen I Testing

Tests were initially completed on Specimen I to determine if the existing IR-UTD technology could be used to detect subsurface flaws in the welded specimen. The IR heaters were used for the testing, imparting heat into the surface of the specimen from a position above the specimen, as shown in Figure 3-4. Results from the initial testing revealed that an indication was observed from the surface-breaking crack at the weld toe as shown in Figure 4-1. The testing did not reveal either of the subsurface weld flaws that were embedded in the specimen.

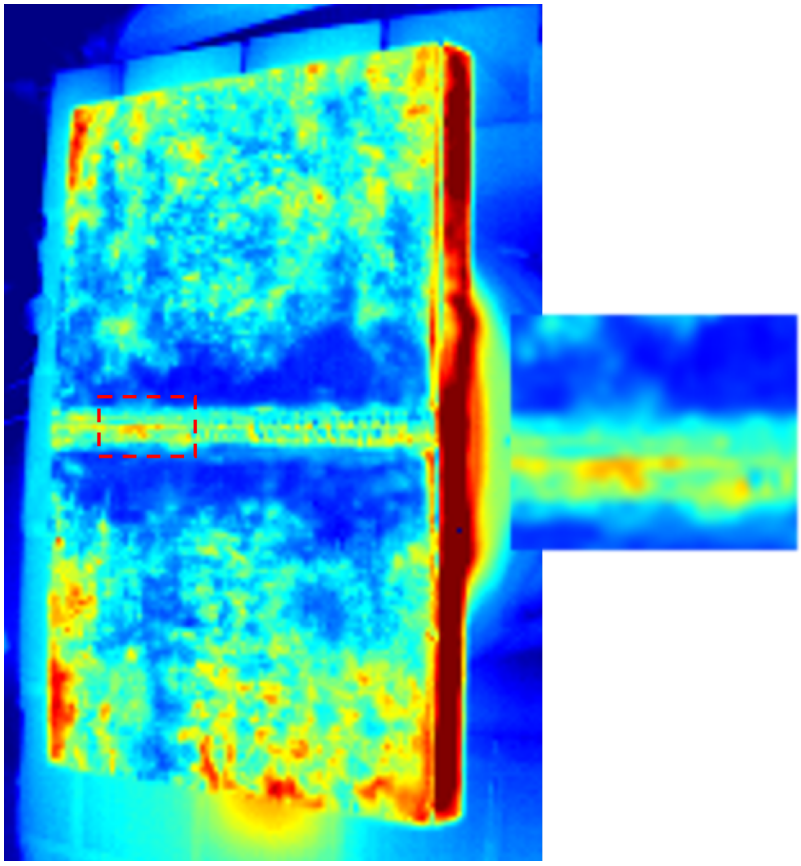

Figure 4-1. IR-UTD image from showing anomaly in the toe crack in Specimen I.

Specimen 1 was also tested using test setup 3, which consisted of mounting a resistive heating element on the surface of the specimen to produce a thermal gradient across the plate. Using this arrangement, the surface crack in Specimen 1 was clearly detectable as shown in Figure 4-2. As shown in the figure, the position of the indication detected in the weld is at the correct location along the weld toe, and extends approximately the same length as indicated for the weld toe crack in the design

drawings (Figure 3-1). The primary defect indication was approximately 0.40 in. in length, and is located approximately 3.2 in. from the edge of the plate, as shown in the figure. This matches the length and position indicated on the design drawings.

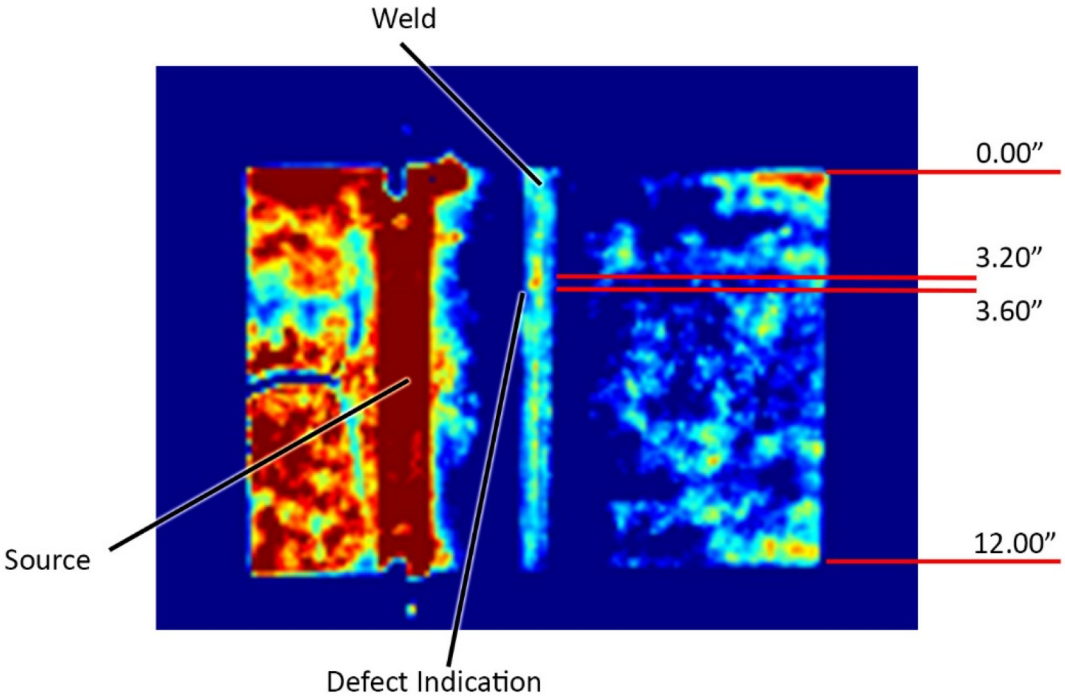

Figure 4-2. IR-UTD image from showing indication in the toe crack in Specimen I.

Figure 4-3 shows the thermal distribution on the surface of the plate during the heating and cooling process. Figure 4-3A shows the thermal output from individual pixels in the thermal image. The location of the individual pixels in the image are shown in Figure 4-3B. The pixels in sound areas of the plate were labeled 1,2 and 3. The pixel from the same location as the crack in Specimen I was labeled 0. The vertical axis in Figure 4-3A shows the output from an individual pixel, and the horizontal axis shows time. As shown in this figure, the resistive heating element produced a thermal gradient in the surface of the plate. For example, pixel 1 shows the largest output because it is closest to the heating source. Pixel 2 shows a reduced thermal output, and pixel 3 shows a thermal output smaller than pixel 2 because it is further from the heat source. The pixel captured at the location of the defect has a greater output than pixel 3, even though it is furthest from the heating source. These data indicate quantitatively that the heat flow is disrupted by the presence of the surface-breaking defect, affecting the thermal output detected by the individual pixels. As a result, the crack appears as an indication in the processed IR-UTD image. In a conventional IR image, produced without the time-lapse processing implementing in the IR-UTD, the indication does not appear clearly because of the noise created by other surface anomalies such as the irregular surface of the weld and the weld toe.

Repeatability tests were also conducted to determine if the indication could be accurately reproduced in different tests. Figure 4-4 shows the results from three separate tests in which a thermal gradient was produced in the plate by use of the resistive heater, and thermal images were captured using the IR-UTD technology. As shown in this figure, the surface-breaking crack indication was consistently produced during these tests.

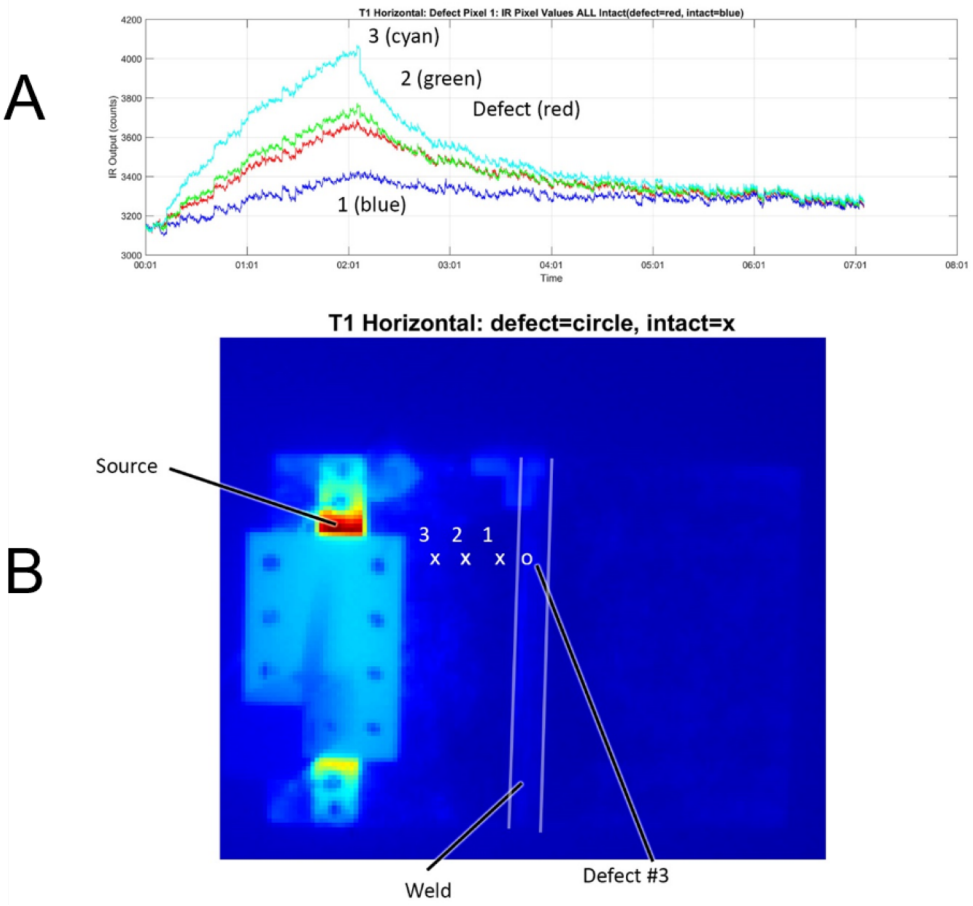

Figure 4-3. Thermal output from individual pixels (A) and a conventional thermal image of Specimen I (B).

Additional testing was conducted on Specimen I utilizing IR coating inspection system (IR-CIS). The IR-CIS is a similar to a PPT system, utilizing a pair of flash lamps to deposit a small amount of thermal energy on the surface of the specimen. This system was developed for detecting defects under coatings such as paint and metalizing. The results of the tests did not produce indications from the surface-breaking toe crack or the subsurface defects in the weld. A contributing factor to the IR-CIS not producing useful results included the reflectivity of the surface of the steel, and the small amount

of thermal energy deposited on the surface as a result. Consequently, further testing of this technology was not pursued.

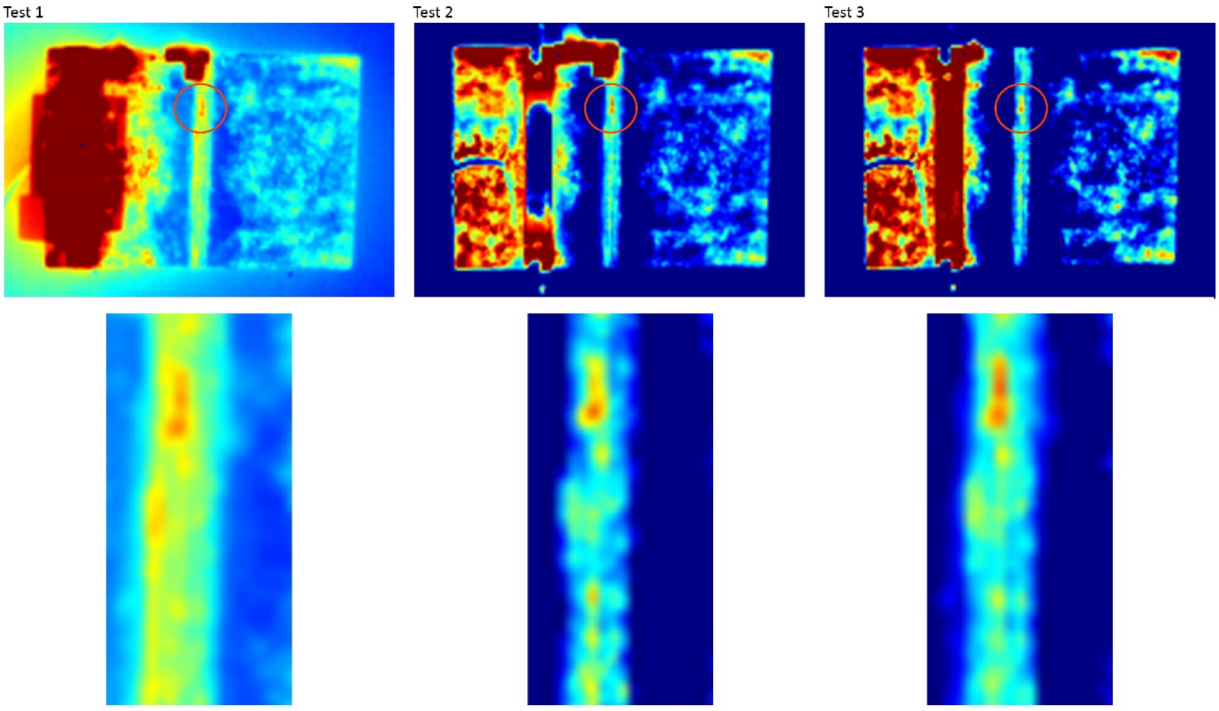

Figure 4-4. Results of repeatability tests showing the toe crack indication in Specimen I.

It was concluded from the initial testing that an improved test setup was needed that allowed for both the camera and the IR heaters to be normal to the surface of the plate. Test setup 2 was developed to meet this need. Results from test setup 3 confirmed that improved image quality was observed with the camera normal to the surface of the specimen. In addition, because the weld flaws were not observed in the testing, it was determined that mock-up specimens with idealized subsurface flaws were needed. These mock-up specimens were needed to provide a basis for investigating different procedures to determine if there were improvements that could be made such that subsurface defects could be detected. This allowed for the potential development of procedures that were more likely to produce useful results in the field. Specimens II and III were fabricated to provide suitable test articles for development. Generally, these specimens included slots and FBHs to simulate subsurface defects as shown in Figures 3-2 and 3-3.

4.2. Specimen II Testing

Specimen II was tested with a variety of different test arrangements, as shown in Table 3-1. Different temperature profiles were implemented to evaluate the different processing approaches being explored through the research, including LT, PPT, and IR-

UTD processing. Figure 4-5 shows example surface temperature cycles that were implemented. Figure 4-5(A) shows a single heating and cooling cycle that was used for evaluating the IR-UTD and PPT processing approaches. Figure 4-5(B) shows cyclical heating and cooling cycles that was used for evaluating the LT, PPT, and IR-UTD approaches.

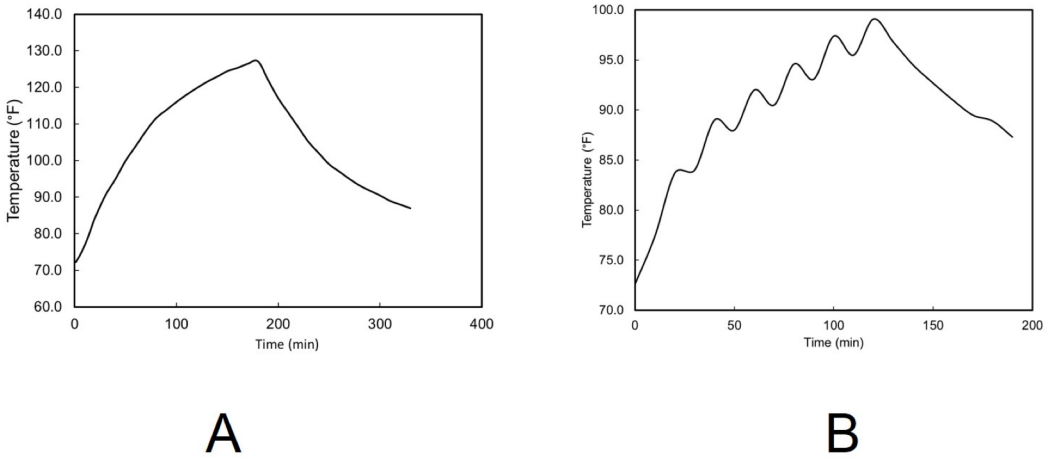

Figure 4-5. Examples of typical surface temperature profiles showing (A) a single heating and cooling cycle and (B) cyclical heating and cooling cycles.

It was found from the testing of Specimen II that the subsurface FBHs and slots at depths of 0.20 or greater did not produce indications in any of the tests. Specimen III was subsequently fabricated with flat-bottom holes with depth of 0.2 in. and less. Specimen III, which had FBHs at depths of as little as 0.05 in. from the surface being imaged by the IR cameras, was intended to provide more easily detectable features to provide a basis for the development of procedures.

4.3. Specimen III Testing

Specimen III is a 0.25-in. thick plate with FBHs with depths ranging from 0.050 to 0.20 inches. This plate was tested using the electrical IR heaters, laboratory oven, and gas heaters as excitation sources. Infrared electrical heater tests did present results showing indications associated with the subsurface FBHs.

Specimen 3 was placed in a laboratory oven and heated to ~300°F. The specimen was removed from the oven and placed within the test frame for imaging. Data was collected during the cooling process. The observation of the specimen during the

cooling process from a high temperature was intended to simulate the cooling of a weld. Data was evaluated using the IR-UTD processing scheme. The FBHs did not produced indications that could be detected.

Specimen III was also tested using propane heaters as shown in Figure 4-6. Figure 4-7 shows the surface heating and cooling cycle for a test using the gas heaters. The high-capacity gas heaters provided for a much more rapid increase in temperature of the surface as compared with the electric IR heaters. A surface temperature increase of 45°F was achieved using the gas heaters, based on measurements from a thermocouple mounted on the surface of the plate, as shown in Figure 4-7. The rate of heating was ~ 3°F per minute during the heating portion of the cycle, and ~ 1.5°F per minute during the cooling cycle.

The data from the tests were processed using IR-UTD, PT, and LT processing approaches. Both the heating and the cooling portion of the cycle was used for analysis of results.

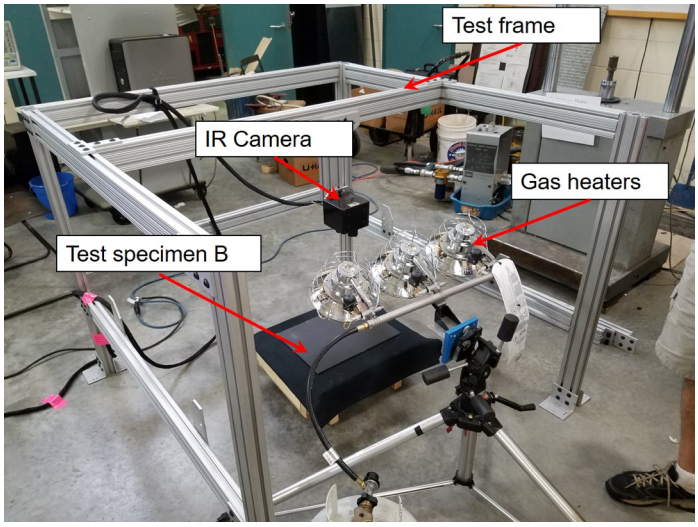

Figure 4-6. Test setup for heating the surface of Specimen III with gas heaters.

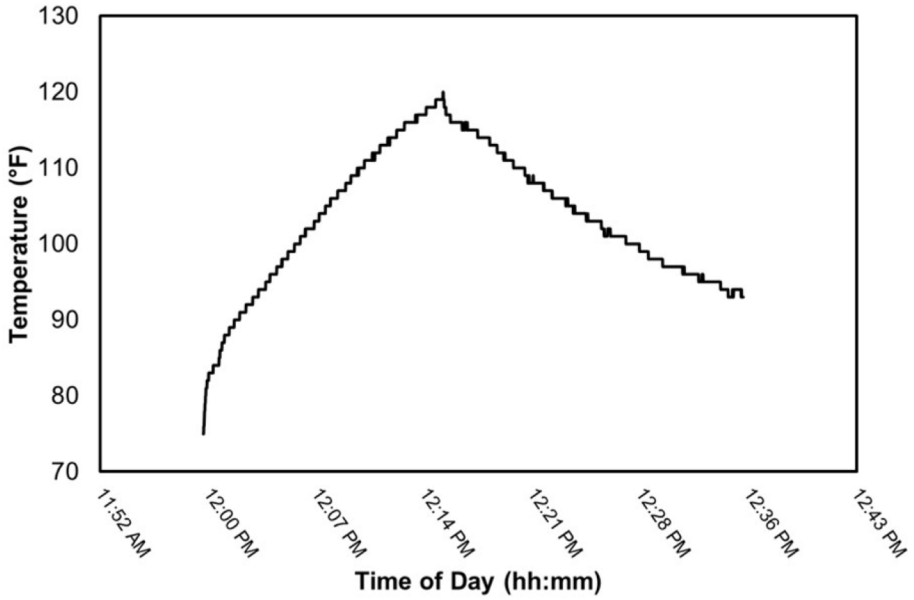

Figure 4-7. Surface heating and cooling cycle using gas heaters.

The results of the testing of Specimen III using the propane heaters showed that four of the subsurface FBHs produced detectable indications. These indications were produced using the IR-UTD processing approach. Figure 4-8 shows the IR-UTD image in which four of the eight FBHs can be observed. Three indications were observed for the row of 0.5 in. diameter FBHs, including FBHs at depths of 0.05, 0.01, and 0.015 in. below the surface of the specimen. A 0.25 in. FBH at a depth of 0.010 in. also produced a slight indication. As shown in the image, gradients on the surface of the specimen were present that make interpretation of the image more difficult. The gradient is represented in the image by a dark area impinging on the image from the top edge of the plate and the white areas near the bottom of the plate. Improvement of the

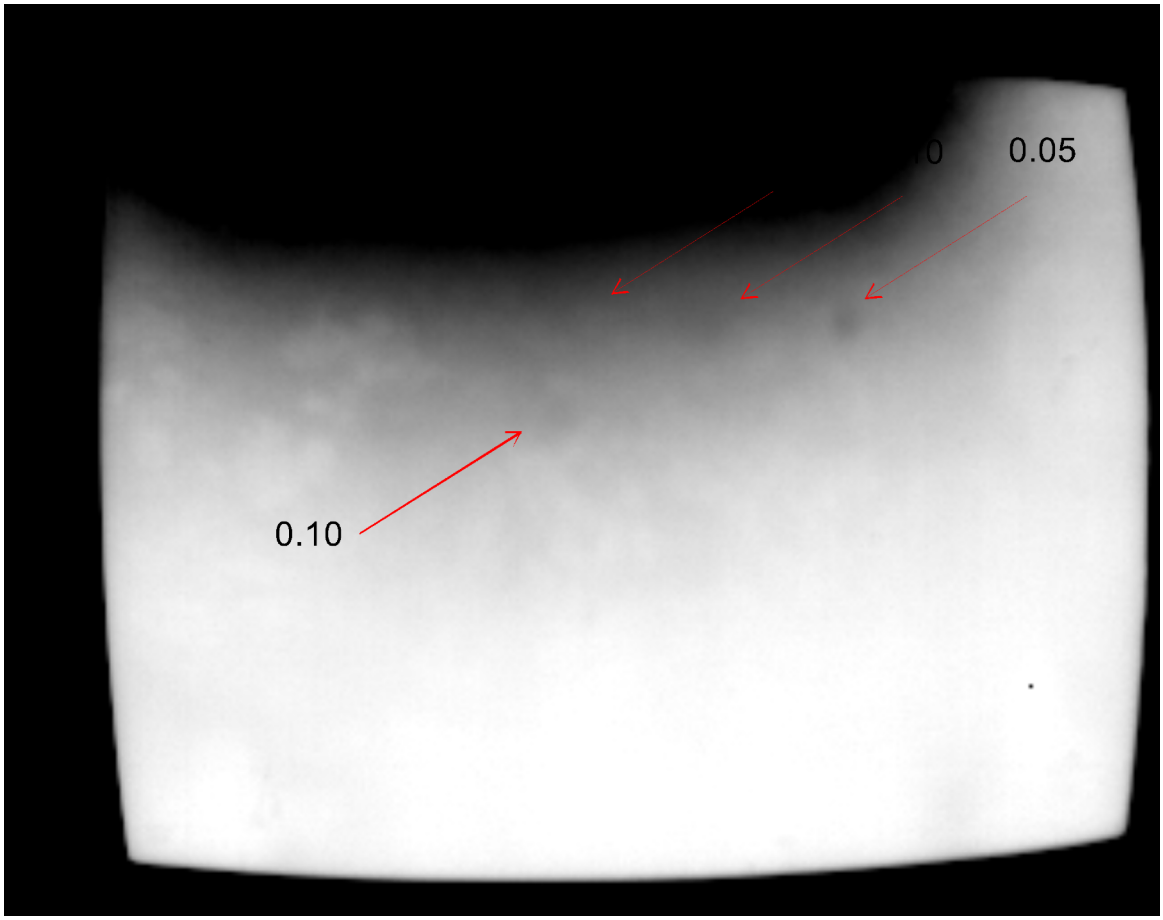

Figure 4-8. IR-UTD test results showing indications from flat-bottom holes with depths of 0.05 in, 0.10 in and 0.15 in.

excitation source to present a more uniform temperature distribution on the surface of the specimen may improve the quality of the image.

The indications produced by the FBHs can be difficult to observe in static images such as that shown in Figure 4-8. Dynamic adjustment of the scaling is needed to more easily observe the indications. These data were analyzed to provide quantitative demonstration of the anomalies observed in the IR-UTD data and represented in Figure 4-8. The analysis consisted of evaluating the actual pixel values from the data represented in the image, to identify anomalies in the area of the FBH as compared with sound areas of the metal plate. Data from a line bisecting the FHBs were normalized to nearby pixel values in the sound are of the plate, to reduce the effect of the gradient in the image and identify anomalies associated with the FBHs. Figure 4-9 shows the results of the analysis, showing that the FBHs produced measurable anomalies in the data. The horizontal axis in the figure is the distance across the plate in millimeters. Red circles are placed at the spatial location of the FBHs in the image, and corresponding anomalies in the data are can be observed at those locations. Interestingly, the 0.20 in. deep FBH appeared to produce a significant anomaly in the quantitative data, though was not apparent in the image. Regardless, these data

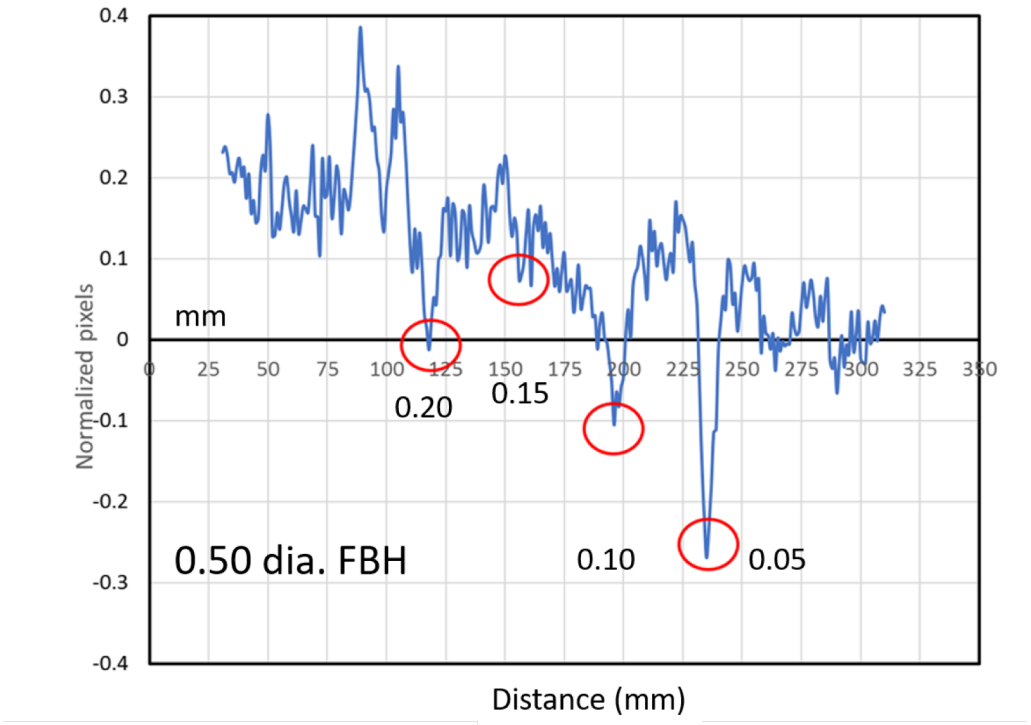

Figure 4-9. Quantitative analysis of data showing anomalies resulting from subsurface FBHs in Specimen III.

indicate anomalies (i.e. indications) at the location of the 0.05, 0.10 and 0.15 in deep FBHs.

The FBHs at a depth of 0.050, 0.10 and 0.15 in also produced indications in the phase image produced by LT processing. Figure 4-6 shows the phase image with arrows

pointing to the areas where indications from the FBHs can be observed in the image. The indications are somewhat difficult to observe in a single static image, and are more apparent with dynamic scaling in the area, as previously noted. It was also found that PPT processing produced indications for the 0.05 in. deep FBH, but improvements to the LT algorithms ultimately produced better results showing indications in the same areas as the IR-UTD processing.

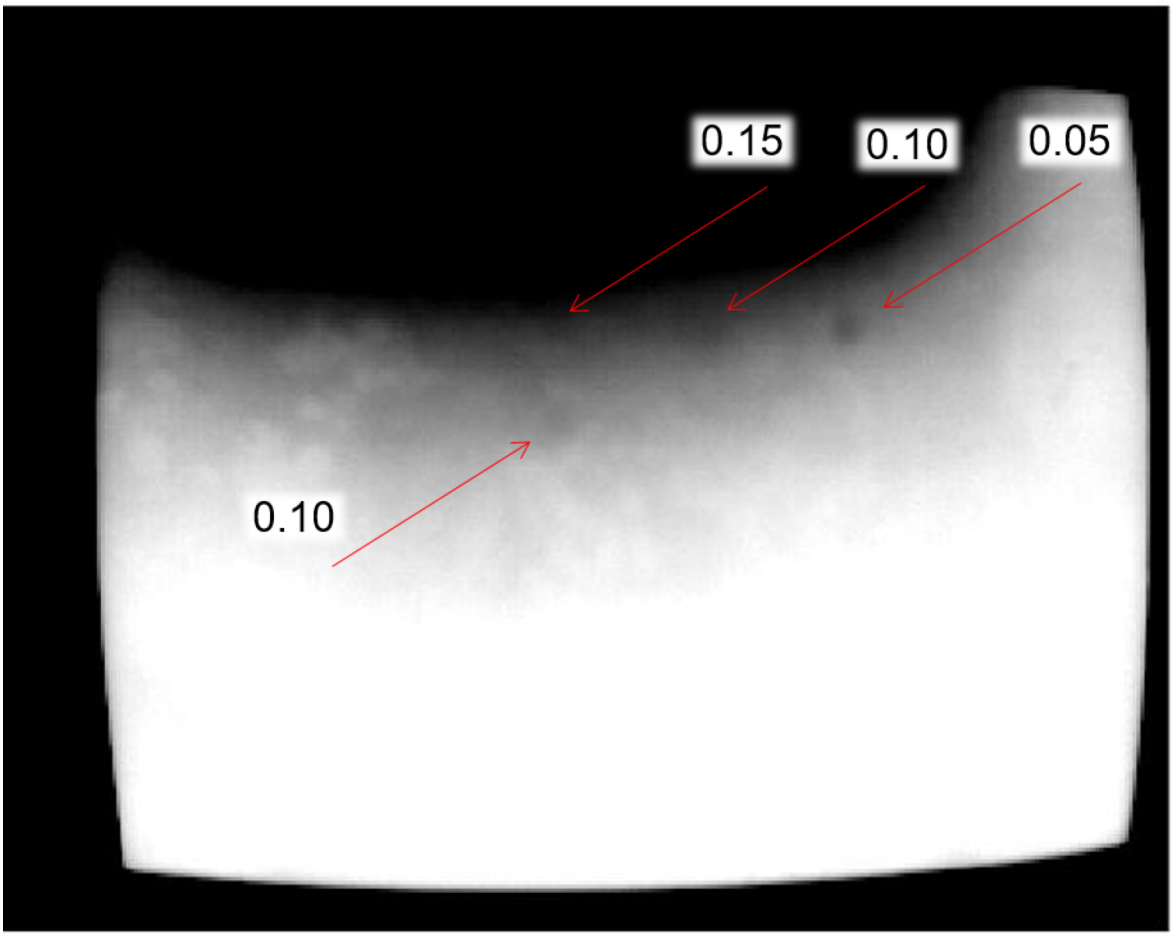

Figure 4-10. Phase image of Specimen III showing subsurface FBH at a depth of 0.050 in from the surface.

The overall results from the laboratory testing indicated that the advanced IRT technologies have limited ability to produce indications from subsurface features in the steel plates. Using a rapid heating process, combined with a normal cooling process,

produced the best results, showing an indication from a 0.15 in. deep, 0.5 in. diameter FBH.

4.4. Welding Observation

Testing was conducted to observe the thermal behavior of a weld during cooling and to collect thermal images capturing thermal behavior during the welding process. The data collected was processed using the IR-UTD algorithms. The testing was conducted at DeLong, Inc., a fabricator located in Jefferson City, MO. During the testing, the submerged metal arc welding process was used to join two flange plates. The welding process joined a plate measuring 1 ½" x 20" into 1 ¾" x 24" plate.

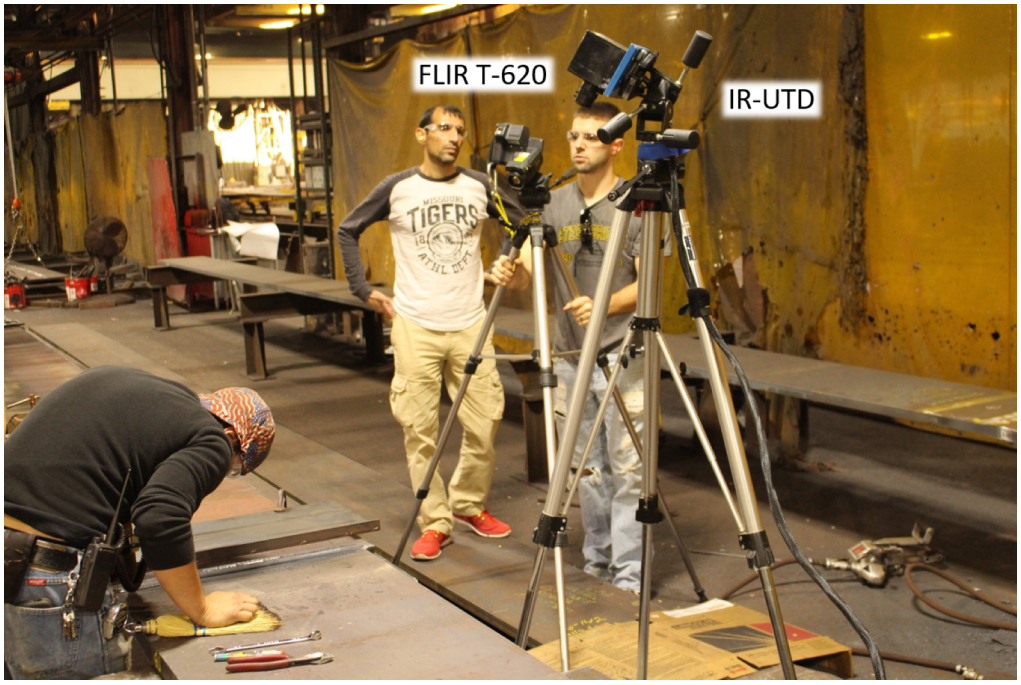

Figure 4-11. Observation of the welding process at DeLong, Inc.

Observations of the thermal response were conducted using two IR cameras, the IR-UTD system and a conventional FLIR T620 hand-held camera. The test arrangement is shown in Figure 4-11. The FLIR 620 camera was used to document the cooling cycle, since it was not possible to mount a thermocouple on the surface of the steel. Additionally, the FLIR camera was placed in a high temperature mode that allowed for data to be collected during the welding process, during which temperatures were above the limit of the IR-UTD camera collecting data with high sensitivity. (When set to collect data at high temperatures, the sensitivity of both the FLIR 620 and the IR-UTD is reduced.) In this way, a complete dataset was collected, although the high-temperature data is collected with lower sensitivity. Data from the FLIR 620 camera was used to produce a temperature record from a location at the toe of the weld shown in Figure 4-

12. The data shown in this figure were captured from the IR spot measurement using the FLIR T620 camera set initially in high temperature mode, and later switched to low temperature mode once the surface had cooled sufficiently. As shown in the figure, data was collected during the welding process and during the cooling of the plates.

The welding was completed with several partial-length passes that resulted in weld termination near the middle of the plate. Figure 4-13 shows a photograph of the weld surface after welding, and partial passes can be observed in the image. This figure shows the condition on the surface of the plate during the thermal monitoring of the cooling process. All flux was removed from the surface of the weld using a brush when welding was completed, and IR images were captured as the plates were cooling.

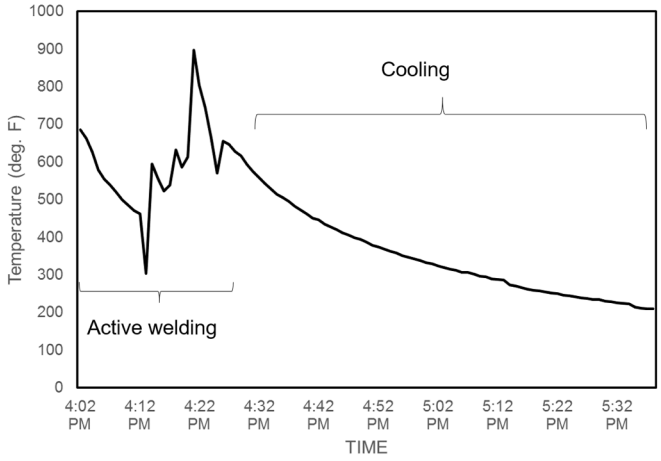

Figure 4-12. Temperature record of active welding and weld cooling.

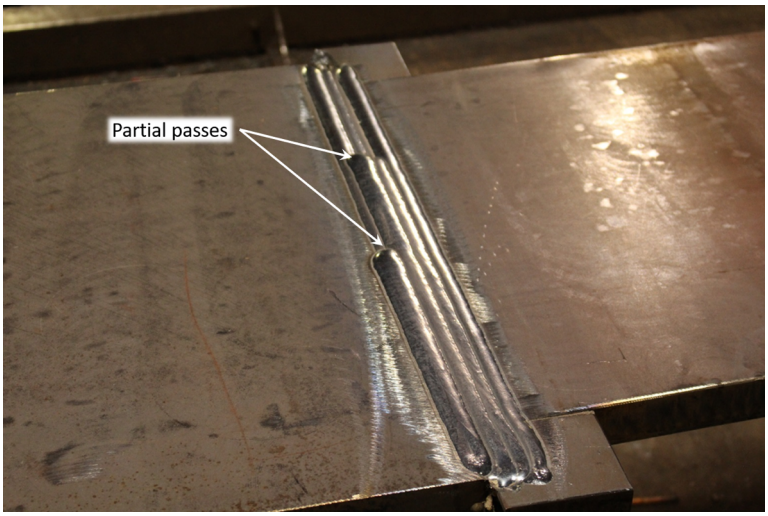

Figure 4-13. Photograph of the weld surface showing partial passes.

Figure 4-14 shows a thermal image captured during weld placement. It can be observed in this image that during the welding process a portion of the weld is concealed by the flux. This flux was removed between separate passes, such that monitoring of the weld for anomalies during the welding process may be a possible means of address the limited depth capabilities found during the laboratory tests. As noted above, all flux was removed using a brush when welding was complete.

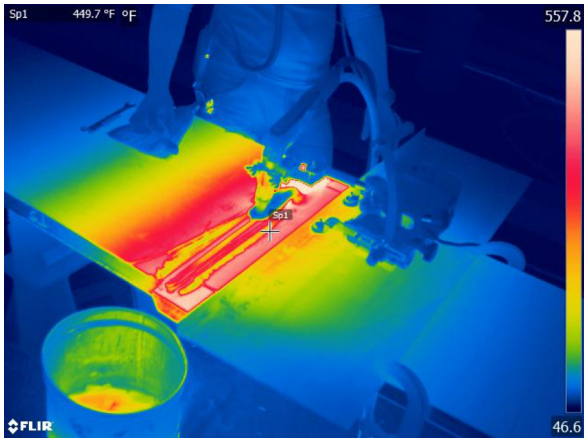

Figure 4-14. Thermal image captured during welding.

The IR-UTD data was analyzed during the cooling of the weld. Figure 4-15 shows the results of the analysis. The figure shows a conventional IR image on the left and the image produced from IR-UTD processing on the right. It can be qualitatively observed

in these data that the IR-UTD data produced appears to have less noise and produces greater indications in the area of the weld terminations as compared with portions of the weld that were placed earlier in the welding process. It can also be observed that the partial-length passes appear in the UTD image because these areas are cooling at a different rate than portions of the weld placed earlier. This has a potential impact of the implementation of the IR-UTD processing, because certain areas of the of the weld were not uniformly heated during the welding process. As shown in the temperature history (Figure 4-12) the rate of cooling is increased at higher temperatures, and diminishes as the steel tends toward thermal equilibrium with the ambient environment. As a result, when there are significant thermal variations due to welds placed at different times, these manifest in the processed data as anomalies that have the potential to obscure indications from defects.

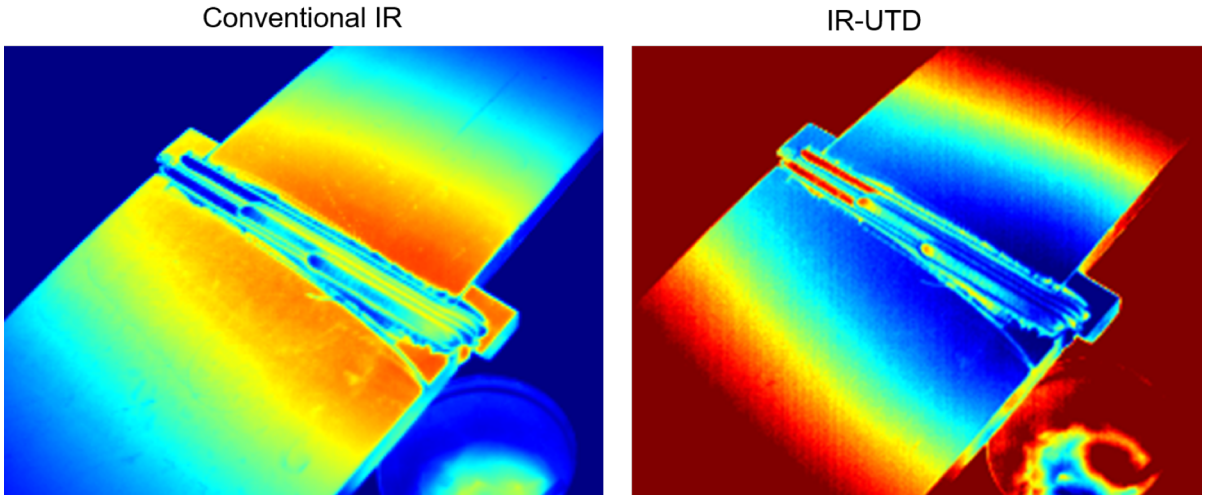

Figure 4-15. Conventional IR image (left) and IR-UTD processed image from weld cooling.

Observations from testing in the fabrication shop included the following:

- There can be significant variations in surface temperature during and after the welding process, undermining the ability of advanced IR methods to identify anomalies in the images associated with defects.
- Imaging of the weld in-between passes could provide an opportunity to evaluate welding during placement. This would reduce the depth requirements for a system to be effective.
- There appeared to be few logistical limitations to monitoring the weld process using thermal cameras. No changes in the procedures typically used by the fabricator were needed to observe the weld using thermal cameras.

The weld that was observed during the reported testing was radiographed. No reportable indications were found in the radiograph.

5. Chapter 5 - Summary

The conclusions from the research were as follows:

1. The IR-UTD technology produced an indication from the 0.40 in. long surface-breaking toe crack in the welded Specimen I. This indication was stronger when a thermal gradient was imposed on the surface of the specimen as compared to uniform heating.
2. Subsurface FBHs were detected at depths of 0.050 in., 0.10 in. and 0.015 in Specimen III.
    a. Improved excitation sources that resulted in increased rates of heating were needed to reveal the subsurface FBHs
    b. IR-UTD processing was capable of producing indications from FBHs at depths of 0.05, 0.10, and 0.15 in.
    c. PPT processing techniques can image the FBH at a depth of 0.050 in.
    d. LT processing was capable of producing indications from FBHs at depths of 0.05, 0.10, and 0.15 in.

Results to date are promising and have shown the IR technology has the capability to detect surface-breaking cracks and subsurface FBHs. Experimental testing is moving in the right direction for improving the quality of images and providing a proof-of-concept for the IR technology. Further work is needed to refine these methods and develop a suitable procedure for detecting volumetric flaws in a weld. Currently, the capability of the technology appears to be limited for detecting subsurface defects to depths of approximately 0.15 in. in steel. Based on the results of the research, the limited depth at which FBHs could be detected indicates that additional research is needed make this technology feasible for shop inspection of groove welds for the purpose of detecting volumetric (subsurface) defects. However, the capability of the technology to detect surface breaking cracks was demonstrated in the research as feasible and currently applicable.

Testing in a fabrication shop was completed in order to gain experience in the shop environment and collect data documenting the cooling process following weld placement. The results from this test indicated that irregularities in the placement of the weld produced thermal anomalies that will challenge the ability to detect subsurface defects in welds. Thermal data from cooling was processed using the IR-UTD technology, and the weld terminations were apparent in these images due to the different cooling rates in these areas. The weld that was observed in the fabrication shop did not have any reportable indications according to a radiograph produced of the weld.

The ability of the technology to detect cracks may have several practical applications in the near term. First, the technology could supplement current procedures relying on radiography for weld inspection. Radiography has limitations in terms of detecting cracks; the non-contact, non-intrusive nature of the advanced IRT could supplement the radiographic results, while being simpler to implement than other technologies such as

phased array ultrasonics. The technology could also potentially be used for inspection of fillet welds, where current requirements include the use of magnetic particle testing. The objective nature of advanced IRT could improve the reliability of the process. The use of advanced IRT could also reduce the operational impact by working on-line during the welding process, such that later testing by magnetic particle would no longer be necessary.

A third potential application of the capability of advanced IRT to detect cracks is for light poles and sign supports. Fillet welds are common in these structures and both radiography and ultrasonics are challenged by the geometry of the welded connections. For example, base plate-pole connections can be difficult to radiograph and complex for ultrasonic inspection. Radiographs of tubular connections require angled configurations and/or multiple images through two walls. The advanced IRT is relatively insensitive to the geometric configuration, and could be used at the time of welding to observe the cooling process and detect crack in the fillet weld or at the weld toe. The technology could also be applied for in-service inspections using a heat source to generate thermal gradients in the material necessary for cracks to be detected. Advanced IR could be used for both aluminum and steel materials.

References

AWS (2010). *Bridge Welding Code AWS D1.5*. Miami, FL, American Welding Society.

Choi, M., Kang, K., Park, J., Kim, W., and Kim, K.(2008). "Quantitative determination of a subsurface defect of reference specimen by lock-in infrared thermography." *NDT & E International* **41**(2): 119-124.

Fuchs, P. A. (2014). *Portable Active Thermographic Coating Inspection System*. Washington, D.C. , United States Department of Transportation.

Ibarra-Castanedo, C., J.M. Piau, S. Guilbert, N. Avdelidis, M. Genest, A. Bendada, and X.P.V. Maldague. (2009). "Comparative study of active thermography techniques for the nondestructive evaluation of honeycomb structures." *Research in Nondestructive Evaluation* **20**(1): 1-31.

Kinzel, A., C. Burgess, and A. Lytle. (1929). "Non-Destructive Testing of Welds by Means of the Stethoscope and X-ray." *Journal of the American Welding Society **8** (9)*: 71-78.

Maierhofer, C., R. Arndt, M. Rollig, C. Rieck, A. Walther, H. Scheel, and B. Hillemeier. (2006). "Application of impulse-thermography for non-destructive assessment of concrete structures." *Cement and Concrete Composites* **28**(4): 393-401.

Maldague, X. (2000). "Applications of infrared thermography in nondestructive evaluation,",in Pramod K. Rastogi and Daniele Inaudi (eds), Trends in Optical Nondestructive Testing and Inspection. Amsterdam, Netherlands: Elsevier. Pp 591-609.

McGonnagle, W. J. (1956). "Some Nondestructive Testing Methods For Testing Welds." *The Welding Journal* **35**(11):1110-1119**.**

Rezai, A., M. Moore, T. Green, and G. Washer (2005). *Laboratory and Field Testing of Automated Ultrasonic Testing (AUT) Systems for Steel Highway Bridges*. FHWA-HRT-04-124 Final Report. Office of Infrastructure Research and Development, FHA. McLean, VA.

Shenefelt, G. A. (1971). "Ultrasonic Testing Requirements of the AWS 1969 Building Code and Bridge Specifications." *The Welding Journal* **50** (5): 342-349.

Washer, G., R. Connor, and D. Looten (2014). "Performance testing of inspectors to improve the quality of nondestructive testing." *Transportation Research Record* 2408: 107-116.

Washer, G., J. Dawson, P. Ruiz-Fabian, A. Sultan, M. Trial, and P.A. Fuchs (2016). *Field Testing of Hand-Held Infrared Thermography*, Phase II TPF-5(247) Final Report. Missouri Department of. Transportation. Jefferson City, MO, University of Missouri.

Appendix - Project Schedule

Task/Deliverable Description	**Anticipated Date of Deliverable Submittal (month/year)**	**TO BE COMPLETED BY RESEARCH CENTER (performance monitoring)**
Kick-off meeting	January 2017	
Deliverable 1 – A written report that contains a review of the literature related to IRT techniques and flaw detection in welds. (Task 1)	June 2017	
Deliverable 2 – A written report that contains a summary of the activities and experiment, analysis of the potential for using IRT for the inspection of welds in steel bridge members, and recommended future research to further develop the technology toward implementation. (Task 2)	September 2017	
Deliverable 3a – Draft final report (Task 3a)	October 2017	
Deliverable 3b – Schedule closeout teleconference (Task 3b)	November 2017	
Deliverable 4 – Final report (Task 4)	January 2018	